PAPER

Four New Eclipsing Binary Systems in the TESS field: CD-34 13220, HD 295082, TYC 6484–426–1 and TYC 6527–2310–1

To cite this article: Burak Ula 2021 *Res. Astron. Astrophys.* **21** 295

View the article online for updates and enhancements.

Research in
Astronomy and
Astrophysics

Four New Eclipsing Binary Systems in the TESS field: CD-34 13220, HD 295082, TYC 6484–426–1 and TYC 6527–2310–1

Burak Ulaş

Department of Space Sciences and Technologies, Faculty of Arts and Sciences, Çanakkale Onsekiz Mart University, Terzioğlu Campus, TR 17100, Çanakkale, Turkey; *burak.ulas@comu.edu.tr*
Astrophysics Research Centre and Observatory, Çanakkale Onsekiz Mart University, Terzioğlu Campus, TR 17100, Çanakkale, Turkey

Abstract We present the first evidence for the binarity of four targets in the TESS field. The temperatures are estimated by SED analysis and the orbital periods are determined. The TESS light curves of the systems are analyzed and the orbital and the absolute parameters are derived. The targets are also compared to well-studied binary systems with the same morphological type and their evolutionary states are discussed. Our results indicate that the stars belong to the class of eclipsing detached binary systems.

Key words: binaries: eclipsing — stars: fundamental parameters — stars: individual: CD-34 13220, HD 295082, TYC 6484–426–1, TYC 6527–2310–1

1 INTRODUCTION

Binary stars are significant stellar objects in the sense of allowing researchers to determine the physical parameters of the components precisely and investigate the stellar evolution of the stars in various circumstances. Ever since Giovanni B. Riccioli's observation of Mizar in the 17th century and Christian Mayer's first catalog of double stars in 1781, astronomers have forged away in understanding the light variation and physical properties of these types of systems. The number of newly discovered binary star systems increased at the beginning of the 1900s, the years when astronomers were keen on finding new systems, as mentioned in Niemela (2001). At the present time, a recently updated version of the Binary Star Database (Kovaleva et al. 2015) consists of about 120 000 stellar systems. A growing number of space-based observations also made a major contribution to the discovery and investigation of the properties of the component stars in detail, thanks to their precise data. Eclipsing binaries, a subclass of binary star systems, are also important tools in astrophysics in understanding the structure and characteristics of the stars. The analyses of the light and radial velocity curves of eclipsing binaries enable us to derive not only the physical parameters like mass, radius, luminosity and temperature but also structural phenomena, for example apsidal motion and atmospheric parameters such as limb darkening and gravity darkening as remarked by Guinan (1993).

Our information on several stellar phenomena, including binarity, was increased by recent space-based missions like Kepler (Borucki et al. 2010) and Transiting Exoplanet Survey Satellite (TESS, Ricker et al. 2015). For instance, the Kepler Eclipsing Binary Catalog (Kirk et al. 2016) consists of light curves and related parameters of 2878 systems. TESS, on the other hand, is very opportune in studying low amplitude variations such as the light curves of pulsating stars in binary systems. The mission focused on the identification of transiting planets around nearby stars by scanning 85% of the sky in its first two years (Ricker et al. 2015). Several parameters of approximately 400 000 selected stars are planned to be cataloged in the TESS Input Catalog (TIC, Stassun et al. 2019). In addition to the above programs, ground-based surveys like the Large Sky Area Multi-Object Fiber Spectroscopic Telescope (LAMOST, Zhao et al. 2012) and the All Sky Automated Survey (ASAS, Pojmanski 2002) provided a great improvement in the discovery and knowledge of the structure and evolution of binary stars. For example, the atmospheric parameters of 2020 EA- and 9149 EW-type binary systems observed by LAMOST were cataloged, and their evolutionary states were discussed by Qian et al. (2018) and Qian et al. (2020); 256 000 binary or variable

star candidates were also detected by Qian et al. (2019) among 786 400 stars falling into the field of LAMOST.

The targets investigated in this study have not been classified as eclipsing binary systems in the literature so far. CD-34 13220 (TIC 277373390) can be found in several catalogs (Thome 1994; National Aeronautics and Space Administration 1993; Morrison et al. 2001; Cutri et al. 2003; Röser et al. 1994; Høg et al. 2000; Gaia Collaboration et al. 2018) which list the position and magnitude information on the stars. Cruzalèbes et al. (2019) list HD 295082 (TIC 42828781) in their Mid-infrared Stellar Diameters and Fluxes Compilation Catalogue with the estimated distance and angular diameter values of 533.2 pc and 0.063 mas, respectively. The star also appears in the Henry Draper Extension Charts (Nesterov et al. 1995) in which the spectral class, position and magnitude values are tabulated. TYC 6484-426-1 (TIC 31303242) is in the photometric empirical calibration research of Ruiz-Dern et al. (2018). They included the star to the list of targets with low extinction by giving $E(B - V)_{\max}$ = 0.0083. Cantat-Gaudin et al. (2018) remarked that TYC 6527–2310–1 (TIC 63192395) does not belong to an open cluster in their study on astrometric parameters of 128 open clusters. The star was also listed among solar-like oscillators in the TESS field by Schofield et al. (2019) which gives fundamental parameters combining the Gaia Data Release 2 (DR2) and Hipparcos data.

The lack of comprehensive studies in the literature motivated us to investigate the systems in detail. In the next section, we give the properties of the data and features of the TESS light curves. The details of the light curve analyses and the results affirming our targets' binarity are explained in Section 3. The last section deals with a discussion of the results, evolutionary status and comparison of the systems to well-known binary stars from previous studies.

2 LIGHT CURVE DATA

The TESS light curves of the systems were acquired from the light curve files that are available through the Mikulski Archive for Space Telescopes (MAST) portal[1]. The files contain data to which the photometric analysis and cotrending were applied (Tanenbaum & Jenkins 2018). The Pre-search Data Conditioning Simple Aperture Photometry (PDC_SAP) flux values (F_i) were extracted from the data files and converted to magnitudes (m_i) by relying on the equation $m_i = -2.5 \log F_i$. The TESS

magnitudes (9.45^m, 9.74^m, 10.14^m and 9.60^m for CD-34 13220, HD 295082, TYC 6484-426-1 and TYC 6527–2310–1, respectively) reported by Stassun et al. (2019) were used during the derivation of the magnitudes. A linear trend as a function of time was also removed from the data of TYC 6484-426-1 and TYC 6527–2310–1. Figure 1 plots the systems' light variations in one orbital period interval. These curves represent the common eclipsing binary type variations.

The depths of the primary and secondary minimums are 0.49^m and 0.35^m for CD-34 13220, 0.63^m and 0.55^m for HD 295082, 0.50^m and 0.45^m for TYC 6484-426-1 and 0.44^m and 0.41^m for TYC 6527-2310-1 respectively. Primary minimums last 3.8^h, 9.8^h, 9.6^h and 8.4^h for CD-34 13220, HD 295082, TYC 6484-426-1 and TYC 6527–2310–1, respectively, while the corresponding durations of the secondary minimums are 3.6^h, 9.1^h, 9.6^h and 8.2^h. The data are from observation sector 13 for CD-34 13220, sector 6 for HD 295082, sectors 5 and 6 for TYC 6484-426-1, and sectors 6 and 7 for TYC 6527–2310–1. Furthermore, the lack of minima times in the literature directed us to calculate times of minimum light for the systems following the method of Kwee & van Woerden (1956). Table 1 lists 92 calculated times of primary and secondary minimums. In the table, TYC 6484 and TYC 6527 refer to TYC 6484–426–1 and TYC 6527–2310–1, respectively.

The shape and characteristics of the light curves verge upon the light variation of a common detached eclipsing binary system. Therefore, detached morphology must be considered during the analyses, as we introduce in the next section.

3 ANALYSES OF THE LIGHT CURVES

One of the most critical parameters to achieve realistic results in the light curve analysis is the effective temperature of the primary component. Since there is very limited information on the systems in the literature, we estimated the temperatures of the primaries by constructing spectral energy distributions (SEDs) through Virtual Observatory SED Analyzer (VOSA, Bayo et al. 2008) for the available photometric data in the VizieR database (Ochsenbein et al. 2000). Parameter-grid search was used to fit the photometric data to achieve the optimized Kurucz atmosphere model (Kurucz 1979). The process was done for each system in the present study and the results were assumed to be the effective temperature of the primary components.

The absence of sufficient knowledge on the orbital properties of systems in the literature led us to determine orbital period values to be applied in the light curve

---

[1] *http://mast.stsci.edu/portal/Mashup/Clients/Mast/Portal.html*

Table 1 Calculated Times of Minimum Light for the Systems

System	BJD-2457000	Type	System	BJD-2457000	Type	System	BJD-2457000	Type
CD-34 13220	1657.169086(5)	I		1677.021844(5)	I		1476.51675(1)	I
	1656.585189(7)	II		1677.605866(7)	II		1483.57357(1)	I
	1658.336961(5)	I		1678.189751(5)	I		1479.96552(1)	II
	1657.753109(9)	II		1678.774260(9)	II		1487.02209(1)	II
	1659.504652(5)	I		1679.357437(5)	I	TYC 6527	1468.81026(1)	I
	1658.920870(7)	II		1679.941601(7)	II		1470.34182(1)	II
	1660.671987(5)	I		1680.525091(5)	I		1471.87524(1)	I
	1660.088789(7)	II		1681.109487(7)	II		1473.40676(1)	II
	1661.840223(5)	I	HD 295082	1470.39149(1)	I		1474.94005(1)	I
	1661.256646(7)	II		1468.91985(1)	II		1476.47153(1)	II
	1663.008070(5)	I		1473.33431(1)	I		1481.06986(1)	I
	1662.424379(7)	II		1471.86274(1)	II		1479.53642(1)	II
	1664.175831(6)	I		1476.27736(1)	I		1484.13472(1)	I
	1663.592091(7)	II		1474.80601(1)	II		1482.60138(1)	II
	1664.760032(7)	II		1479.22043(1)	I		1487.19953(1)	I
	1666.511393(5)	I		1480.69188(1)	II		1485.66590(1)	II
	1665.927797(7)	II		1482.16348(1)	I		1493.32929(1)	I
	1668.847170(5)	I		1483.63491(1)	II		1491.79568(1)	II
	1669.431362(7)	II		1485.10649(1)	I		1496.39400(1)	I
	1670.014987(5)	I		1486.57796(1)	II		1494.86020(1)	II
	1670.599053(7)	II		1488.04936(1)	I		1499.45889(1)	I
	1671.182855(5)	I		1489.52086(1)	II		1497.92537(2)	II
	1671.766854(7)	II	TYC 6484	1441.23240(2)	I		1502.52388(1)	I
	1672.350583(5)	I		1444.68152(1)	II		1500.99050(1)	II
	1672.934813(7)	II		1448.28973(1)	I		1505.58870(1)	I
	1673.518278(5)	I		1455.34646(1)	I		1507.11994(1)	II
	1674.102572(7)	II		1451.73825(1)	II		1508.65350(1)	I
	1674.686146(5)	I		1462.40318(1)	I		1510.18469(1)	II
	1675.270310(7)	II		1458.79505(1)	II		1511.71839(1)	I
	1675.854005(5)	I		1469.45999(1)	I		1513.24959(1)	II
	1676.438160(7)	II		1472.90868(1)	II			

analyses. For doing this, we first employed Fourier analysis to the light curve data of each system using PERIOD04 software (Lenz & Breger 2005) and obtained a frequency value that corresponds to the orbital period. Alternatively, we averaged the differences between consecutive times of minimum light of the same types to estimate a period value. From these two values, the one constructing the better light curve was adopted as orbital period value. Period analyses were also conducted for times of minimum in Table 1 by assuming a linear trend. Variation in time of minimum light (ΔT_0) and orbital period (ΔP) were calculated utilizing the equation $O - C = \Delta T_0 + \Delta P \cdot E$, where E is the cycle number. Results are listed for each system in the last two lines of Table 2 and Figures 4 and 5 are plotted by using the final period values.

The mass ratio is another significant parameter in the light curve analysis, just as temperature and orbital period mentioned in the previous paragraphs. The lack of any research related to the mass ratios of the systems in the literature pointed us to apply the q-search technique to the light curves in order to estimate mass ratio values. Although the shapes of the light curves and the orbital period values imply that the systems are detached binaries, we applied q-search to the systems' binned light curves covering 1500 data points in both detached

and conventional semi-detached mode since there is no information about the morphological classes of the systems in the literature. The difference between $\Sigma(res)^2$ (residual sum of squares) of the solutions with two assumptions confirmed that the systems are detached binaries, as can easily be hypothesized from the light curve shapes even at first glance. The results are presented in Figure 2.

We analyzed the TESS light curves using PHOEBE (Prša & Zwitter 2005) which implements the Wilson-Devinney method (Wilson & Devinney 1971) to solve the light curve and obtain the stellar parameters from input data. Following the results of the q-search, we applied analyses by assuming that the systems are detached binaries. The adjustable parameters are the inclination i, temperature of the secondary component T_2, mass ratio q, surface potential values of both components Ω_1 and Ω_2, and luminosity of the primary component L_1 during the solutions. The albedos ($A_1=A_2=0.5$) are calculated from Ruciński (1969) and the gravity darkening coefficients ($g_1=g_2=0.32$) for the systems were adopted from von Zeipel (1924) and Lucy (1967) by considering the granulation boundary for main sequence stars located at about a spectral type of F0 (Gray & Nagel 1989). Logarithmic limb darkening coefficients (x_1 and x_2) were adjusted from Claret (2017) based on the initial tempera-
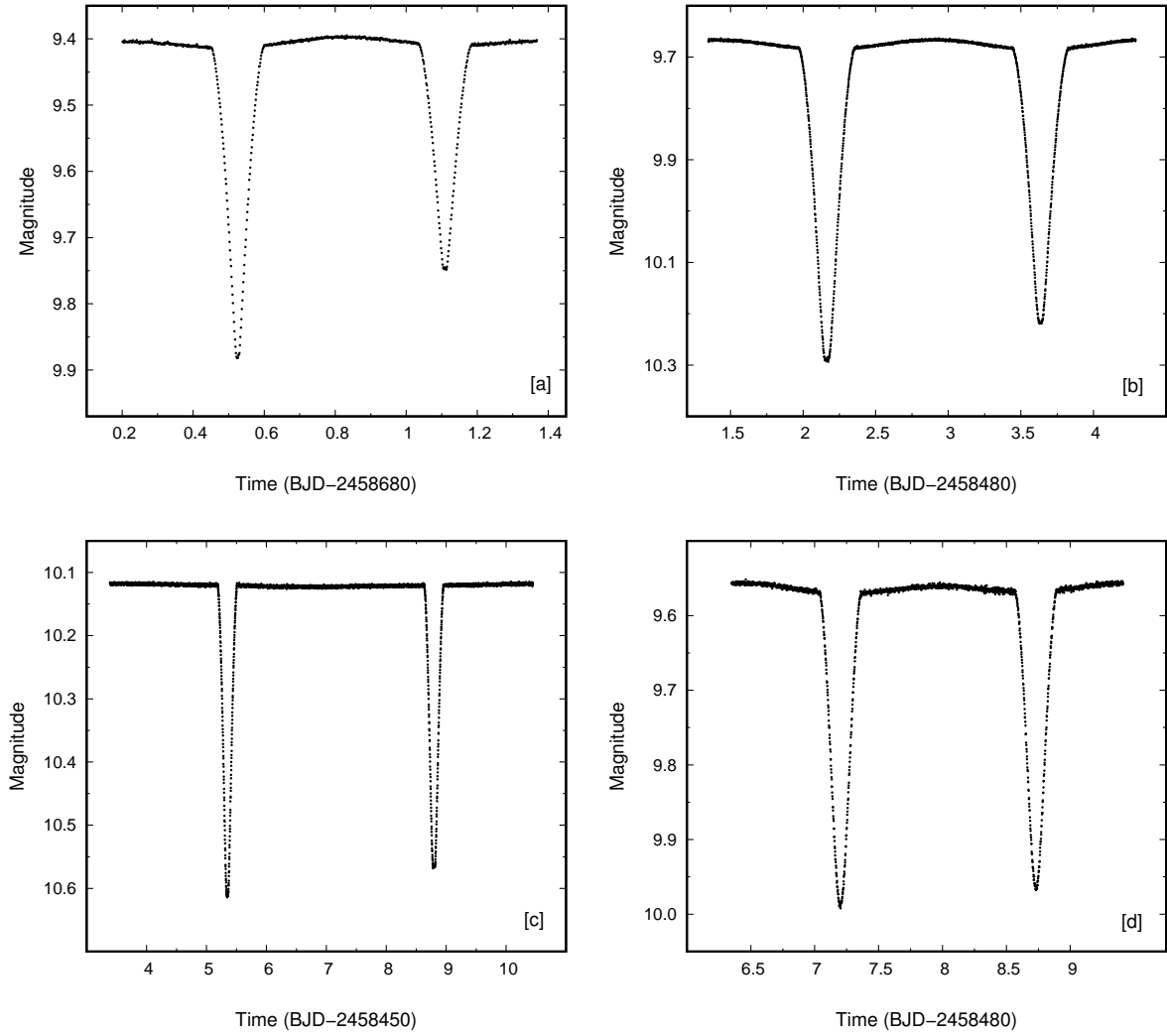
Fig. 1 One-period-long light curves of CD-34 13220 (a), HD 295082 (b), TYC 6484–426–1 (c) and TYC 6527–2310–1 (d). Magnitudes are calculated by referencing the TESS magnitudes reported in Stassun et al. (2019).

tures of the components and are expressed in Table 2. In the table, the uncertainties in T_1 are listed as obtained in SED analyses, 2 450 000 is subtracted from the times of minimum light and, moreover, TYC 6484 and TYC 6527 refer to TYC 6484–426–1 and TYC 6527–2310–1, respectively. The fill-out factors for the components, f, were also calculated by utilizing the relation $f = \frac{r}{r_L}$, where $r_L = \frac{0.49q^{\frac{2}{3}}}{0.6q^{\frac{2}{3}} + \ln(1 + q^{\frac{1}{3}})}$, the volume radius of the Roche lobe, is given by Eggleton (1983).

3.1 CD-34 13220

The temperature of the primary component was derived by SED analysis, as remarked in the previous section. The effective temperature interval was set to 6000-6500 K during the SED analysis, according to the temperatures 6152 K of Gaia Collaboration et al. (2018) and 6345 K

of Stassun et al. (2019). The log g interval was selected as 2.5–5.0 following TIC (Stassun et al. 2019). The extinction, A_ν=0.2246^m, was calculated using the Galactic Dust Reddening and Extinction interface of NASA/IPAC Infrared Science Archive[2]. The results of the SED analysis were T_e=6250±125 and log g=4.50±0.25. Therefore, the initial effective temperature of the primary was taken as 6250 K during the light curve solution. Figure 3 depicts the model fit of the SED analysis.

The light curve analysis was applied on 17 766 data points in detached binary mode with the initial mass ratio value of 0.5 which was yielded by q-search. The orbital frequency was derived as 0.85551 d^{-1} by relying on PERIOD04 which corresponds to 1.1694 d. However, a more appropriate value, 1.167802 d, was found by calculating the average of differences between consecutive
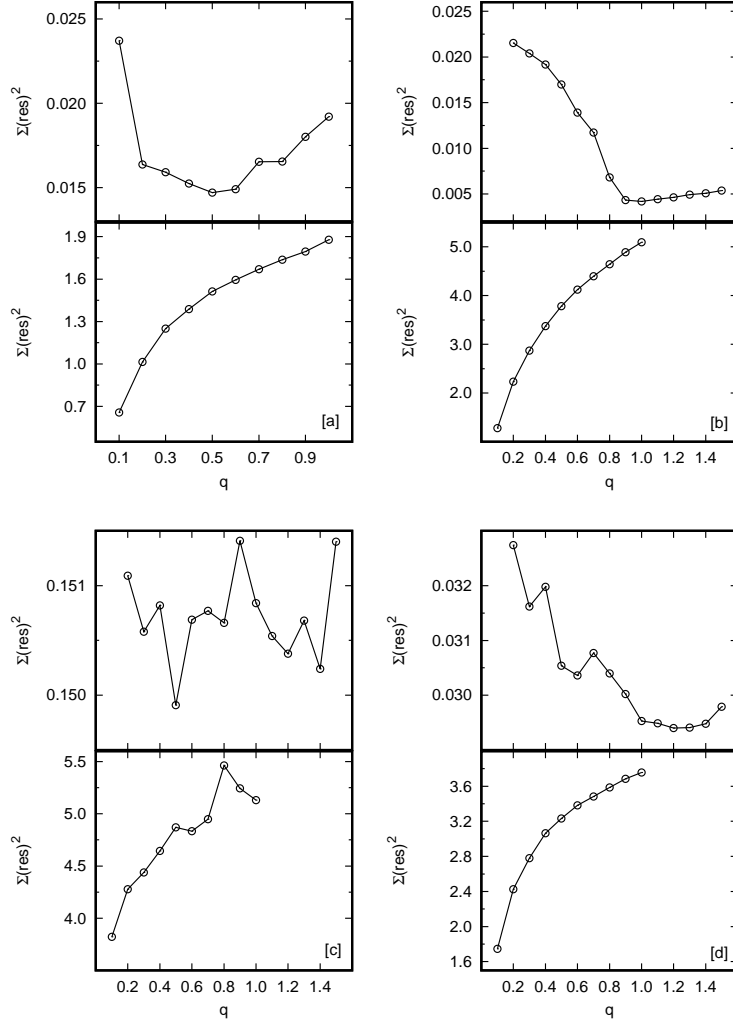
[2] https://irsa.ipac.caltech.edu/applications/DUST/

Fig. 2 Results of the q-searches for CD-34 13220 (a), HD 295082 (b), TYC 6484–426–1 (c) and TYC 6527–2310–1 (d). The upper and lower panels refer to the solutions in detached and semi-detached assumptions respectively.

times of minimum light (see Sect. 3). Moreover, as magnitude difference between two maxima of the light curve exists, the best solution was achieved adopting a spotted area on the secondary component with the parameters of co-latitude $\beta=45°$, longitude $\lambda=270°$, spot radius $r=10°$ and temperature factor $T_f=0.9$. The observations and synthetic light curve are shown together in Figure 4. The resulting light parameters are listed in Table 2.

3.2 HD 295082

Our SED analysis resulted in temperature and surface gravity values of $T_e=6250\pm125$ and log $g=4.00\pm0.25$ respectively. The initial interval of effective temperature was set to 6000–7000 K during the analysis following Gaia Collaboration et al. (2018), Stassun et al. (2019) and F5 spectral type given by Nesterov et al. (1995). The log g interval was 3.0–4.0 considering the value of 3.5 given

Table 2 Results of the Light Curve Analyses

Parameter	CD-34 13220	HD 295082	TYC 6484	TYC 6527
i (°)	82.38(2)	87.78(1)	87.80(1)	84.59(1)
q	0.443(1)	1.001(1)	0.538(1)	1.195(2)
T_1 (K)	6250(125)	6250(125)	6000(125)	6000(125)
T_2 (K)	5904(17)	6055(10)	5970(24)	5936(20)
Ω_1	3.473(9)	6.622(2)	13.30(1)	8.299(6)
Ω_2	3.642(6)	5.459(3)	8.62(1)	6.850(9)
$\frac{L_1}{L_1+L_2}$	0.588(1)	0.4178(2)	0.541(1)	0.338(1)
r_1	0.199(3)	0.1785(7)	0.078(3)	0.141(2)
r_2	0.189(5)	0.226(1)	0.073(3)	0.202(2)
f_1	0.64(1)	0.471(2)	0.24(1)	0.357(5)
f_2	0.61(2)	0.596(3)	0.22(1)	0.512(5)
x_1, x_2	0.586, 0.601	0.583, 0.599	0.595, 0.611	0.597, 0.597
T_0 (BJD)	1657.169086(5)	1470.39149(1)	1441.23240(2)	1468.81026(1)
P (d)	1.167802(3)	2.9430013(9)	7.056833(1)	3.064855(2)

r_1 and r_2 refer to the fractional radii. The standard deviations, 3σ, for the last digits of light parameters are given in parentheses.

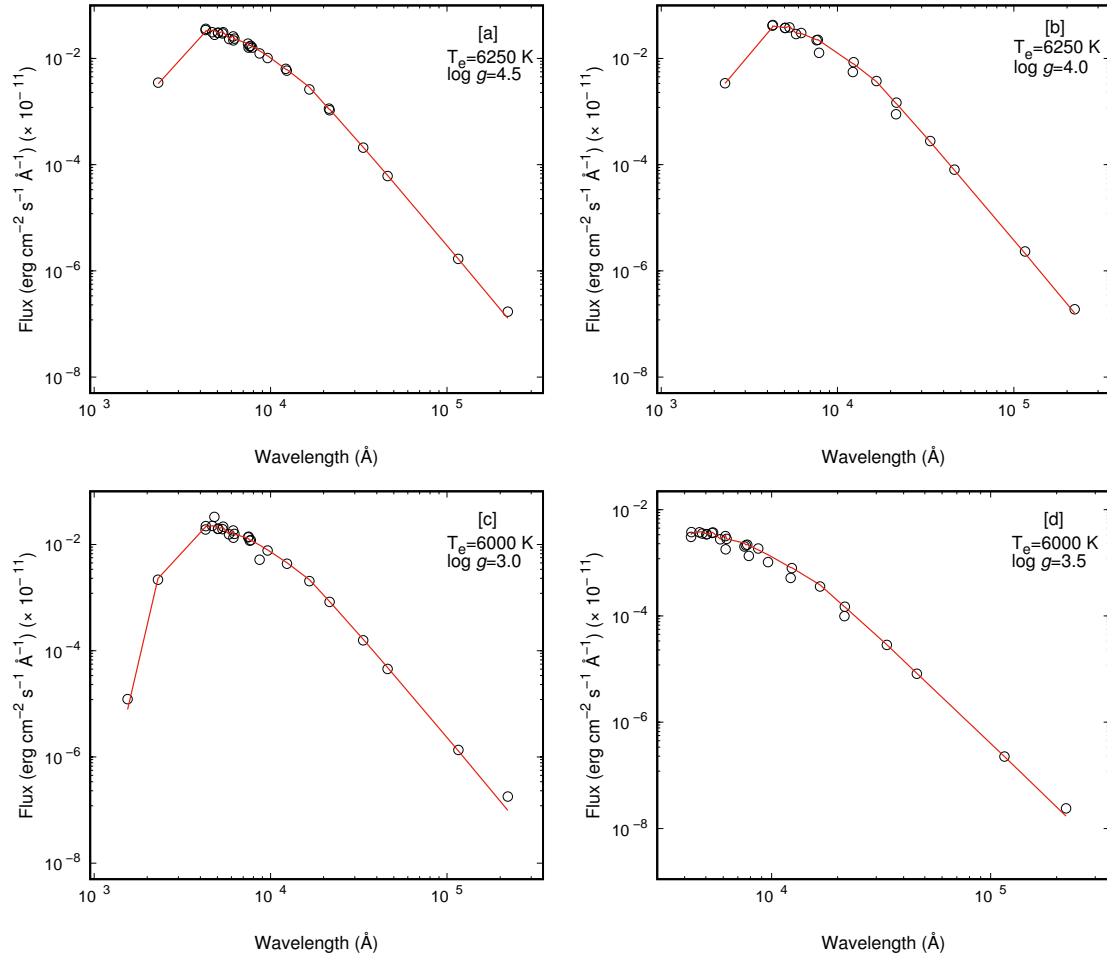by TIC (Stassun et al. 2019) and the visual extinction was

Fig. 3 Results of the SED analyses for CD-34 13220 (a), HD 295082 (b), TYC 6484–426–1 (c) and TYC 6527–2310–1 (d). Open circles indicate the photometric flux values from the VizieR database (Ochsenbein et al. 2000) and the solid (*red in color version*) lines refer to the model fit. Final effective temperature and log g values are expressed in the upper right of each figure. Please note that the axes are on a logarithmic scale.

derived as 1.0618^m. The fit of the SED analysis is plotted with the photometric data in Figure 3.

The light curve analysis was conducted with 14 831 data points composing the light curve. During the analysis, the initial value of mass ratio was taken as 1.0, the result of our q-search. The orbital frequency was found to be $0.3352\,\mathrm{d}^{-1}$ (2.9832 d) and 2.9430013 d by using two methods in Section 3. The latter one was adopted as period value through the light curve solution process. The agreement between the theoretical light curve and observations is displayed in Figure 4. The final parameters found by the analysis are given in Table 2.

3.3 TYC 6484-426-1

The SED analysis ended up with the values of T_e=6000±125 and log g=3.00±0.25 based on the initial interval of 6000–6250 K and 3.0-4.0 for the effective temperature and surface gravity, respectively, following the

values published by Gaia Collaboration et al. (2018) and Stassun et al. (2019) (Fig. 3).

The analysis was applied to the light curve which consists of 31 924 data points. The initial mass ratio was 0.5 and the calculated value of the orbital period is 7.056833 d. Different from our other three targets, the eccentricity was also set as a free parameter during the solution, and it was found to be e=0.0540(6). The synthetic light curve is plotted with the observational data in Figure 5 and the results are tabulated in Table 2.

3.4 TYC 6527-2310-1

The temperature of the primary component was assumed to be 6000±125 K and the log g is 3.50±0.25, the results of the SED model fit. The SED analysis was applied by using the initial parameters of the effective temperature between 5750 and 6000 K and gravity between 3.0 and 5.0 by following values of Gaia Collaboration et al. (2018),
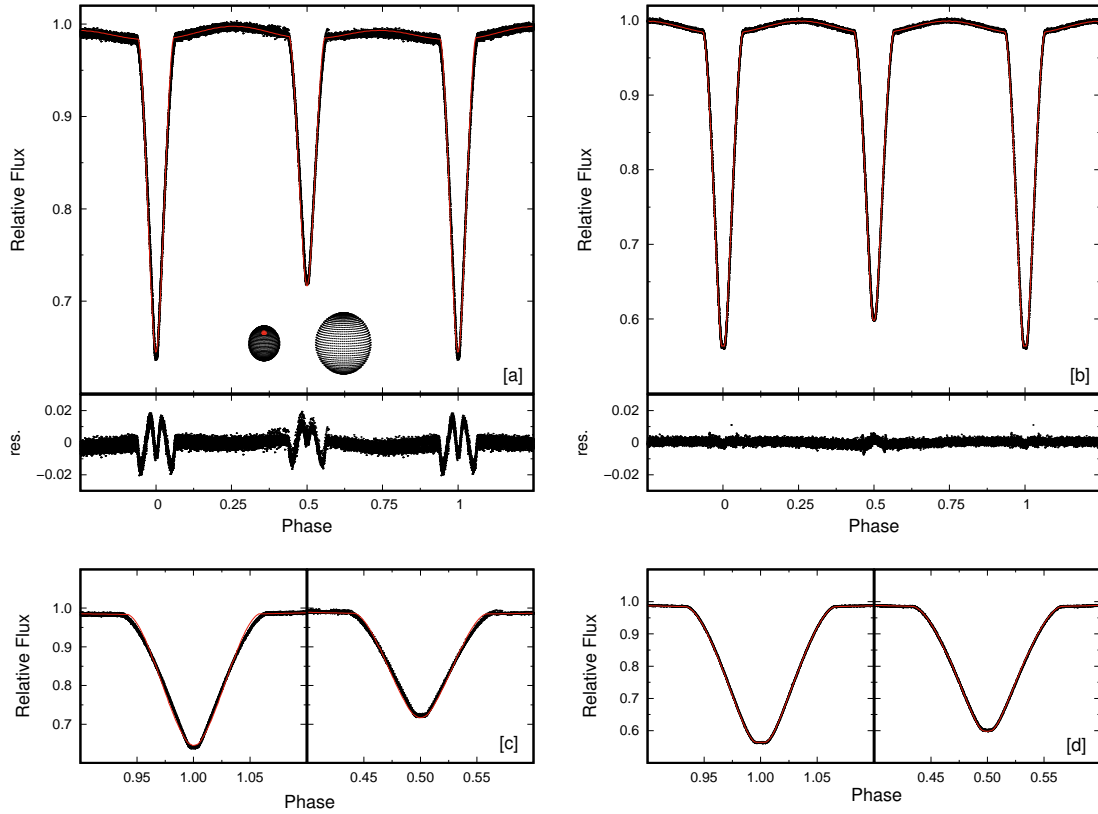
Fig. 4 Observational data with the synthetic light curves (red in color version) of CD-34 13220 (a) and HD 295082 (b). The agreements of the fits are also shown at primary and secondary minimums for CD-34 13220 (c) and HD 295082 (d). The geometry of CD-34 13220 at phase 0.75 is also presented in (a) for visibility of the spotted area (*red*) on the secondary component.

Schofield et al. (2019) and Stassun et al. (2019). The result is plotted with photometric data in Figure 3.

In this process, 31 191 data points were analyzed during the light curve solution with the initial mass ratio value of 1.2 from the q-search. The orbital period was derived as 3.064855 d. Results indicate that the secondary component is more massive and luminous than the primary one as displayed in Table 2. Observational and synthetic light curves are plotted in Figure 5.

We also investigated the solar-like oscillation candidacy of the star, as it was included in the asteroseismic target list of Schofield et al. (2019). Although the temperature of the target (6250 K) can be considered as close to solar temperature, the period analyses conducted with PERIOD04 did not result in any frequency close to 3 mHz, the frequency of the highest amplitude oscillation of the Sun. Therefore, we do not confirm the probable oscillational behavior of the star based on our analysis.

4 CONCLUSION

We present the first results demonstrating that the systems in question are detached binaries. The effective temperature and log g values were estimated for primaries by considering model fits from the SED analyses. The orbital periods were determined by applying frequency analysis and calculating the average of the differences between consecutive times of minimum light. The q-search technique was utilized to estimate the initial values of mass ratios. The TESS light curve solutions indicated that the systems are detached eclipsing binaries. Unlike the other systems, a better fit was achieved by assuming a spotted area on the secondary component of CD-34 13220. We calculated the absolute parameters of the components of systems considering our analysis results by using ABsParEB software (Liakos 2015) which are listed in Table 3. The masses of the primary components were estimated by relying on the stellar tracks for solar abundances of Bertelli et al. (2009) based on their log g and effective temperature. We conclude that the components of HD 295082 have very close mass and radius values while the secondary component of TYC 6527–2310–1 is more massive and luminous than the primary. The results implied that CD-34 13220 and TYC 6484–426–1 are typical detached binary systems.

The four systems were compared to 162 well-known detached binaries cataloged by Southworth (2015). In
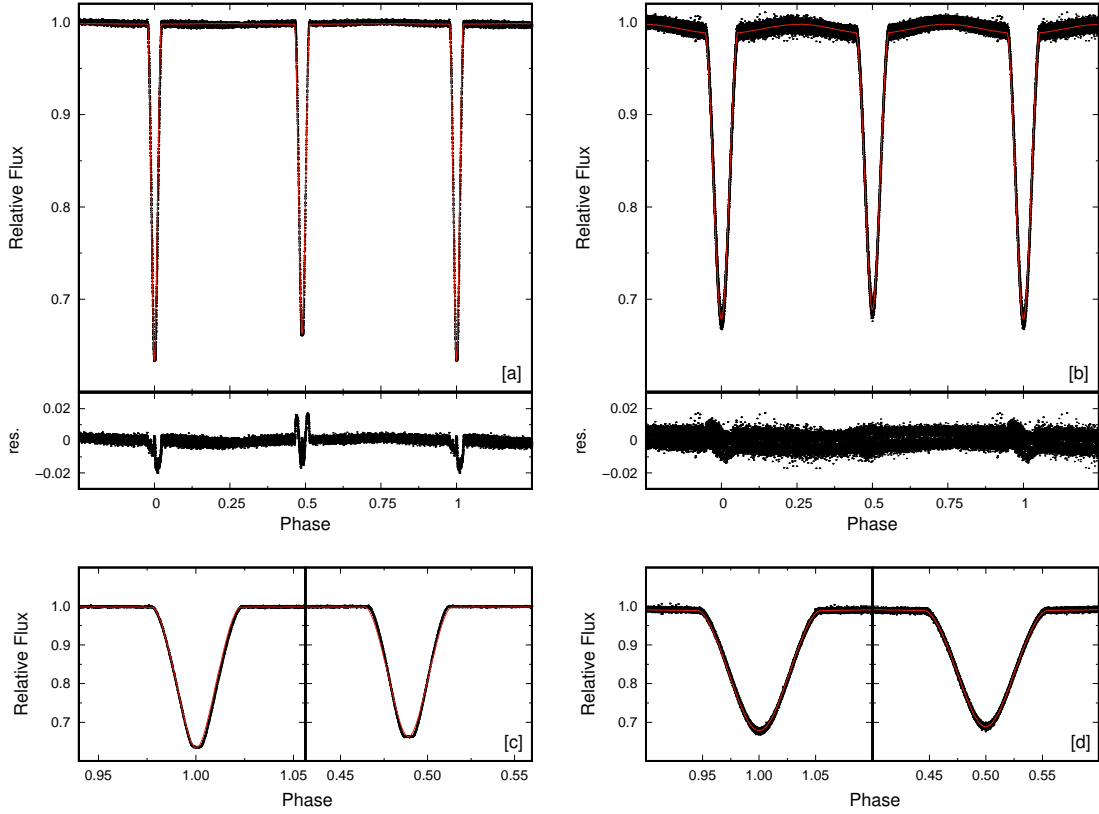
Fig. 5 Same as Fig. 4, but for TYC 6484–426–1 (a and c) and TYC 6527–2310–1 (b and d).

Table 3 Absolute parameters of the systems. TYC 6484 and TYC 6527 refer to TYC 6484–426–1 and TYC 6527–2310–1, respectively. The standard errors are expressed in parentheses for the last digits.

Parameter	CD-34 13220	HD 295082	TYC 6484	TYC 6527
M_1 ($M_\odot$)	1.2	1.3	2.5	1.8
M_2 ($M_\odot$)	0.532(1)	1.301(1)	1.345(3)	2.151(4)
R_1 ($R_\odot$)	1.14(5)	2.17(3)	1.9(5)	2.0(1)
R_2 ($R_\odot$)	1.08(9)	2.74(3)	1.8(6)	2.90(8)
L_1 ($L_\odot$)	1.8(2)	6.4(5)	4(2)	4.8(7)
L_2 ($L_\odot$)	1.3(2)	9.1(8)	4(2)	9.4(9)
a ($R_\odot$)	5.736(4)	12.165(5)	24.83(1)	14.367(9)

general, the locations of the components are in agreement with the other detached binary systems on the mass-radius plane and the Hertzsprung-Russell diagram (Fig. 6). However, it must be pointed out that the secondary component of CD-34 13220 is found to be slightly less massive according to its radius. The components of TYC 6484–426–1 almost overlap on the Hertzsprung-Russell diagram because of their similarity in temperature and luminosity. The locations of the systems are also plotted with the six evolutionary tracks of Bressan et al. (2012) for masses from $0.9\,M_\odot$ to $1.4\,M_\odot$ in Figure 7. The components of the systems seem to follow the evolution of the stars, having initial masses between 0.9 and $1.4\,M_\odot$. The figure also indicates that the secondary components

of HD 295082 and TYC 6527-2310-1 are more evolved than the primaries which led us to consider the possibility of enhanced stellar winds discussed by Tout & Eggleton (1988). The authors focused on mass inversion in RS CVn binaries and indicated that the secondary (originally less massive) component demonstrates tidally enhanced mass loss by stellar wind. They also propose three different evolution scenarios based on the Roche lobe overflow (RLOF) phase and period-mass ratio relation. Although the system Z Her used by authors in their model exhibits some more distinctive properties than our systems in terms of differences between radii and luminosities of the components, our derived mass ratios, and the mass values agree with those of the model star. According to their classification criteria based on final period and mass ratio, HD 295082 and TYC 6527–2310–1 are in the group of systems whose RLOF stage begins at $q > 0.7$ and causes rapid mass transfer through common envelope evolution. We remark that the enhanced stellar wind mechanism is within the realm of possibility in describing the evolved status of secondary components. However, the hypothesis needs to be confirmed by detailed stellar models which reveal the initial orbital period and the masses of the systems.

We compared our targets to LAMOST EA-type eclipsing binaries whose properties are reported by
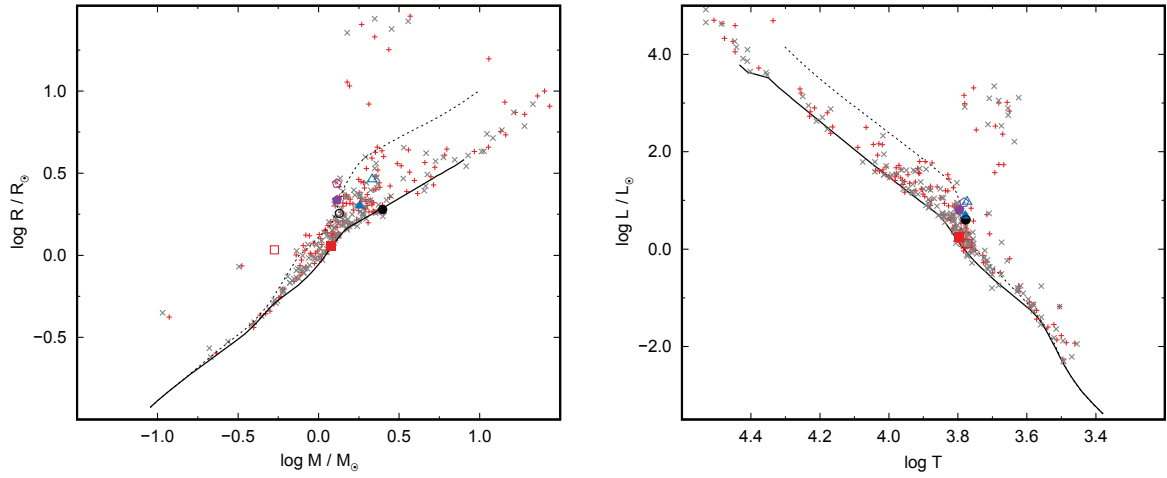
Fig. 6 Locations of the components of the systems on the mass-radius plane (*left*) and the Hertzsprung-Russell diagram (*right*). Pluses and crosses (*pale colors; grey and tan in color version*) refer to the primary and secondary components of known detached systems given by Southworth (2015). Filled signs signify the primary components of the systems, where the open signs correspond to the secondaries. Squares (*red*), pentagons (*purple*), circles (*black*) and triangles (*blue*) refer to the components of CD-34 13220, HD 295082, TYC 6484–426–1 and TYC 6527–2310–1, respectively. The data for ZAMS (*thick solid line*) and TAMS (*dashed line*) with $Z = 0.01$ and $Y = 0.267$ abundance are taken from Bressan et al. (2012).
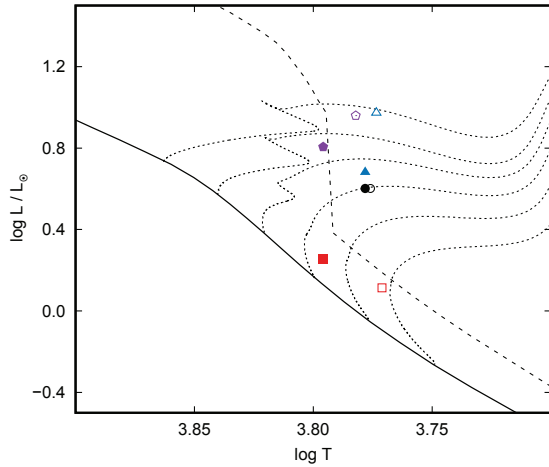
Fig. 7 Components of the systems on the Hertzsprung-Russell diagram with the evolutionary tracks for stars with solar abundances and having the masses of 0.9 $M_\odot$, 1.0 $M_\odot$, 1.1 $M_\odot$, 1.2 $M_\odot$ 1.3 $M_\odot$ and 1.4 $M_\odot$ (*dotted lines, from bottom to top*). The other symbols are the same as those displayed in Fig. 6. The evolutionary tracks, ZAMS (*solid line*) and TAMS (*dashed line*) data for $Z = 0.01$ and $Y = 0.267$ composition are adopted from Bressan et al. (2012).

Table 4 Summary of the box plots of LAMOST EA-type binaries. Temperature and period values are given in K and d, respectively.

	Temperature	Period	$\log g$
Number of data	2956	2906	2956
Lower quartile ($Q1$)	5560	0.9063	4.03
Median ($Q2$)	6130	1.7671	4.15
Upper quartile ($Q3$)	6620	4.3571	4.28
Minimum	3970	0.2909	3.66
Maximum	8210	9.5240	4.65
IQR	1060	3.4508	0.25

targets. These box plots indicate that the temperatures of the components of our systems are in good agreement with the same type of LAMOST stars. The orbital periods of CD-34 13220, HD 295082 and TYC 6527–2310–1 are in the interquartile range (IQR) as well. However, derived $\log g$ values deviate from the IQRs. The five-number summary of box plots is listed in Table 4 with the number of data and IQRs which were calculated by using the equation $IQR = Q3 - Q1$. Additionally, it is planned to inspect a relation among the given properties of LAMOST binaries (i.e. temperature, period, $\log g$, metallicity and radial velocity) and compare to those of our targets. However, a correlation matrix (Fig. 9) constructed utilizing a Python code based on data from 2906 LAMOST EA binaries implied that the parameters are weakly connected (the correlation coefficients are between –0.31 and 0.1) to end up with reliable results. As a consequence, our results suggest that the systems are expected to follow two different evolutionary courses as remarked by Qian et al.

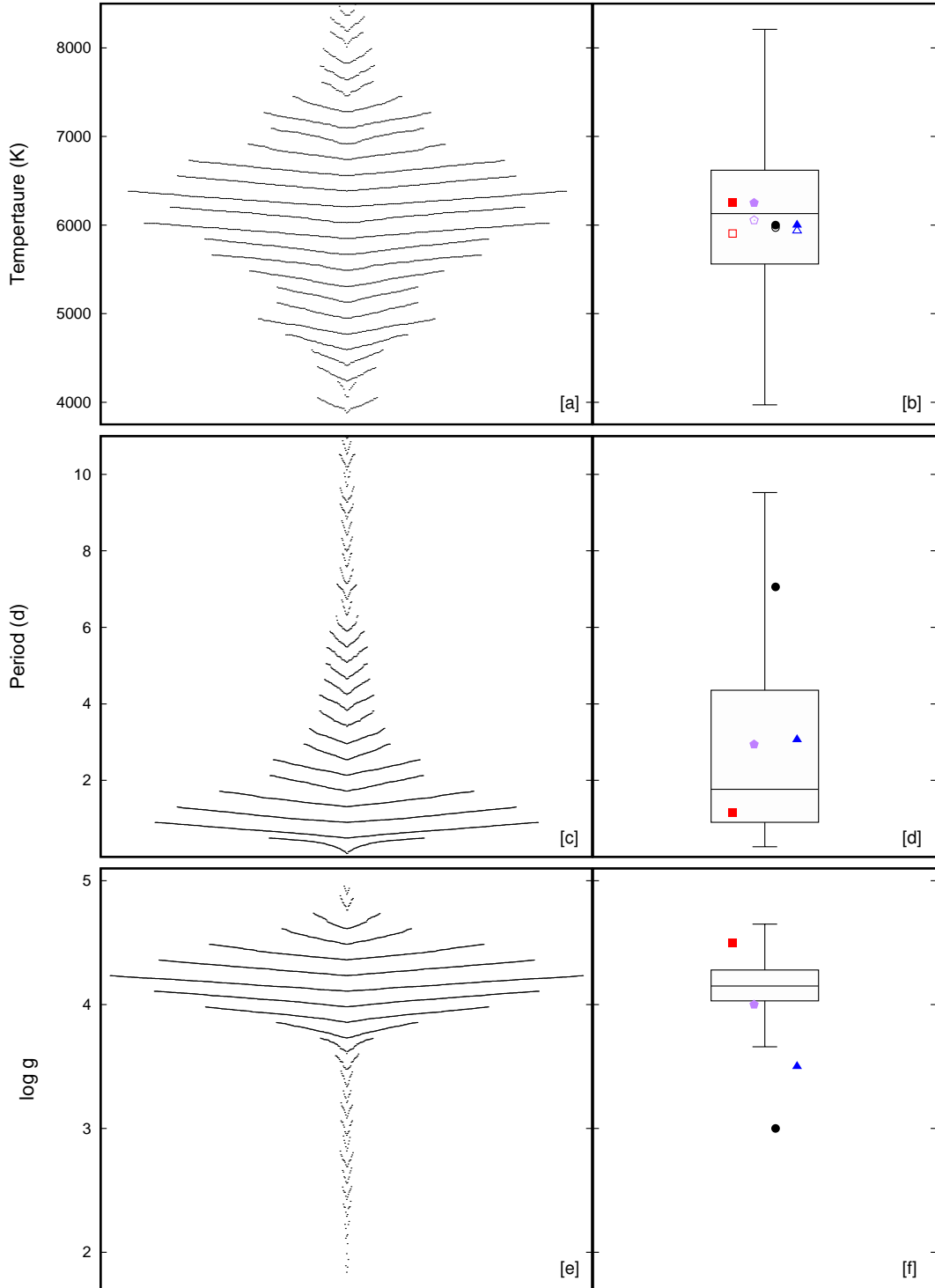Qian et al. (2018). The distribution of the temperatures, orbital periods and $\log g$ values of LAMOST EA binaries are depicted in Figure 8. We also draw box plots (Krzywinski & Altman 2014) of those three distributions (right panels of Fig. 8) to display the variation of the data and to examine its agreement with the parameters of our

Fig. 8 Temperature (a), orbital period (c) and log g (e) distributions of EA-type LAMOST stars based on data from Qian et al. (2018) with their corresponding box plots (b, d and e) where our targets are also flagged. Period values are plotted between 0 and 11 d (c) for the sake of clear visibility, although box (d) is calculated using the whole data interval. The symbols are the same as those shown in Fig. 6. See text for details.

(2018); CD-34 13220 follow the evolutionary path from short-period EA system to less massive EW-type binary through angular momentum loss. The other three long-period systems, on the other hand, are expected to evolve into long-period, massive EW-type binaries via case A mass transfer.

We plausibly conclude that the systems are eclipsing detached binary systems. Advanced spectroscopic obser-
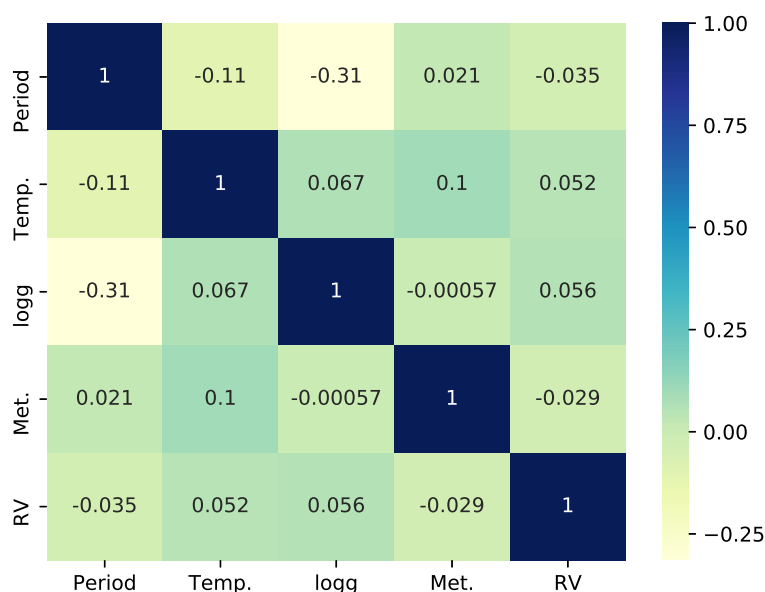
Fig. 9 Correlation matrix constructed based on parameter data of LAMOST EA stars published by Qian et al. (2018). Temp., Met. and RV stand for temperature, metallicity and radial velocity respectively.

vations are needed for a more precise determination of the binary properties of the systems and to confirm the results presented in this study.

References

Bayo, A., Rodrigo, C., Barrado Y Navascués, D., et al. 2008, A&A, 492, 277

Bertelli, G., Nasi, E., Girardi, L., & Marigo, P. 2009, A&A, 508, 355

Borucki, W. J., Koch, D., Basri, G., et al. 2010, Science, 327, 977

Bressan, A., Marigo, P., Girardi, L., et al. 2012, MNRAS, 427, 127

Cantat-Gaudin, T., Vallenari, A., Sordo, R., et al. 2018, A&A, 615, A49

Claret, A. 2017, A&A, 600, A30

Cruzalèbes, P., Petrov, R. G., Robbe-Dubois, S., et al. 2019, MNRAS, 490, 3158

Cutri, R. M., Skrutskie, M. F., van Dyk, S., et al. 2003, VizieR Online Data Catalog, II/246

Eggleton, P. P. 1983, ApJ, 268, 368

Gaia Collaboration, Brown, A. G. A., Vallenari, A., et al. 2018, A&A, 616, A1

Gray, D. F., & Nagel, T. 1989, ApJ, 341, 421

Guinan, E. F. 1993, in Astronomical Society of the Pacific Conference Series, 38, New Frontiers in Binary Star Research, eds. K.-C. Leung, & I.-S. Nha, 1

Høg, E., Fabricius, C., Makarov, V. V., et al. 2000, A&A, 355, L27

Kirk, B., Conroy, K., Prša, A., et al. 2016, AJ, 151, 68

Kovaleva, D., Kaygorodov, P., Malkov, O., et al. 2015, Astronomy and Computing, 11, 119

Krzywinski, M., & Altman, N. 2014, Nature Methods, 11, 119

Kurucz, R. L. 1979, ApJS, 40, 1

Kwee, K. K., & van Woerden, H. 1956, Bull. Astron. Inst. Netherlands, 12, 327

Lenz, P., & Breger, M. 2005, Communications in Asteroseismology, 146, 53

Liakos, A. 2015, in Astronomical Society of the Pacific Conference Series, 496, Living Together: Planets, Host Stars and Binaries, eds. S. M. Rucinski, G. Torres, & M. Zejda, 286

Lucy, L. B. 1967, ZAp, 65, 89

Morrison, J. E., Röser, S., McLean, B., Bucciarelli, B., & Lasker, B. 2001, AJ, 121, 1752

National Aeronautics and Space Administration. 1993, Cape Photographic Durchmusterung, 3

Nesterov, V. V., Kuzmin, A. V., Ashimbaeva, N. T., et al. 1995, A&AS, 110, 367

Niemela, V. 2001, in Revista Mexicana de Astronomia y Astrofisica Conference Series, 11, 23

Ochsenbein, F., Bauer, P., & Marcout, J. 2000, A&AS, 143, 23

Pojmanski, G. 2002, Acta Astronomica, 52, 397

Prša, A., & Zwitter, T. 2005, ApJ, 628, 426

Qian, S. B., Zhang, J., He, J. J., et al. 2018, ApJS, 235, 5

Qian, S.-B., Zhu, L.-Y., Liu, L., et al. 2020, RAA (Research in Astronomy and Astrophysics), 20, 163

Qian, S.-B., Shi, X.-D., Zhu, L.-Y., et al. 2019, RAA (Research in Astronomy and Astrophysics), 19, 064

Ricker, G. R., Winn, J. N., Vanderspek, R., et al. 2015, Journal of Astronomical Telescopes, Instruments, and Systems, 1, 014003

Röser, S., Bastian, U., & Kuzmin, A. 1994, A&AS, 105, 301

Ruciński, S. M. 1969, Acta Astronomica, 19, 245

Ruiz-Dern, L., Babusiaux, C., Arenou, F., et al. 2018, A&A, 609, A116

Schofield, M., Chaplin, W. J., Huber, D., et al. 2019, ApJS, 241, 12

Southworth, J. 2015, in Astronomical Society of the Pacific Conference Series, 496, Living Together: Planets, Host Stars and Binaries, eds. S. M. Rucinski, G. Torres, & M. Zejda, 164

Stassun, K. G., Oelkers, R. J., Paegert, M., et al. 2019, AJ, 158, 138

Tanenbaum, P., & Jenkins, J. M. 2018, TESS Science Data Products Description Document, EXP-TESS-ARC-ICD-0014 Rev D

Thome, M. J. 1994, VizieR Online Data Catalog, I/114

Tout, C. A., & Eggleton, P. P. 1988, MNRAS, 231, 823

von Zeipel, H. 1924, MNRAS, 84, 665

Wilson, R. E., & Devinney, E. J. 1971, ApJ, 166, 605

Zhao, G., Zhao, Y.-H., Chu, Y.-Q., et al. 2012, RAA (Research in Astronomy and Astrophysics), 12, 723